Inclusion of Interbar Currents in a Network-Field Coupled Time-Stepping Finite-Element Model of Skewed-Rotor Induction Motors

S. L. Ho, H. L. Li, and W. N. Fu

Abstract— **In order to include the interbar currents of skewed-rotor inductor motors in finite-element analysis, a three-dimensional (3-D) model is usually necessary. In this paper a two-dimensional multislice time-stepping finite element method of skewed-rotor induction motors is presented to solve such complicated 3-D problems. It is shown that the network of the rotor cage is coupled to finite-element equations so that the interbar currents in the rotor can be taken into account. By arranging the unknowns and mesh-current equations ingeniously, the resultant coefficient matrix of the global system equations are made symmetrical. Compared with 3-D finite-element methods, the computation time for solving field equations with the proposed method is significantly shorter. The model can be used to estimate the high-order harmonic stray losses in induction motors. A comparison between computed and tested results is also given.**

Index Terms—**Finite element methods, induction motors.**

I. Introduction

INDUCTION motors are one of the most widely used machines to convert electrical energy to mechanical energy. Many researchers have studied their performances using finite-element methods (FEM). Most analyses were limited to two-dimensional (2-D) due to its simplicity compared with its three-dimensional (3-D) counterpart [1]. Williamson, in his review paper [2] presented in 1994, pointed out that if 2-D models are used, the following attributes of a real machine, due to its inherently 3-D nature, were still difficult to study accurately:

1) the stator end windings;
2) the rotor end rings;
3) rotor skew (if present);
4) radial ventilation ducts (if present);
5) interbar currents.

Due to the advance in 2-D time stepping FEM in recent years, it is now possible to couple external circuit equations into the global system equations to have a more precise analysis. One can now partially take the effect of the stator end windings and the rotor end rings into account by including the end-winding resistances and inductances [3]–[4].

Manuscript received October 6, 1998; revised April 26, 1999. This work was supported by the Research Committee of the Polytechnic University.

The authors are with the Department of Electrical Engineering, Hong Kong Polytechnic University, Kowloon, Hong Kong, China (e-mail: eeslho@polyu.edu.hk).

Publisher Item Identifier S 0018-9464(99)07598-6.

In order to deal with the problems of skewed rotor bars, a 2-D multislice model has been developed [5]. A set of nonskewed 2-D models, each corresponding to a section taken at different positions along the axis of the machine, is used to model the skewed rotor. In order to ensure that the current flowing in the bars of one slice is the same as that flowing in the bars of every other slices of the same rotor bar, one could carry out the field solutions simultaneously for all the slices. Piriou *et al.* [6] used this method to simulate a permanent magnet synchronous machine. Gyselinck *et al.* [7] used the multislice method to simulate the steady-state operation of a squirrel cage induction motor. Boualem *et al.* [8] also used the multislice approach to simulate the operation of a squirrel cage induction motor. This model was further developed by the authors so that the formulas of the 2-D multislice model is very similar to that of normal 2-D FEM, and the work to develop the software could be simplified [9].

To tackle the problems involving the interbar currents of skewed rotor cage motors, the authors have presented a 3-D time stepping FEM model [10]. A 2-D multislice FEM was coupled into the 3-D model when determining the stator current and the reluctivity of the iron material at each time step. With such approach the 3-D model was reduced into a current driven linear problem, thereby simplifying the system equations considerably to result in big savings in computation time.

However, compared to 2-D models, the 3-D models still need a large amount of computation time in solving practical problems. The computation required in the pre- and post-processing of 3-D FEM data is also complex. It would be highly desirable if 2-D models can be applied.

In this paper a new multislice time stepping FEM model which couples the network circuits of the rotor cage into system equations is presented. The interbar currents can be included by introducing the interbar resistances in the network. By choosing the unknowns and mesh-current equations ingeniously the resultant coefficient matrix of the global system equations becomes symmetrical and the interbar currents can either be included or excluded easily in the program according to user's option. The investigated domain can span one pole or one pair of poles. With the proposed algorithm most induction motors which have no radial ventilation ducts can be solved using this model, although 3-D FEM is still necessary to compute the end-winding impedances if very high accuracy in studying the end-winding fields is required.

0018–9464/99$10.00 © 1999 IEEE

Authorized licensed use limited to: Hong Kong Polytechnic University. Downloaded on March 14, 2009 at 10:34 from IEEE Xplore. Restrictions apply.

The proposed method has been used to estimate the interbar loss of an 11 kW skewed rotor induction motor. A comparison between the results using the 2-D FEM and the 3-D FEM is given. The method is also further used to estimate the high-order harmonic stray losses. A comparison between computed and tested results will also be reported.

II. Basic Equations at Each Domain

The following assumptions are made:

1) there are no leakage fluxes in the outer surface of the stator core and in the inner surface of the rotor core;
2) because the iron cores are laminated, the eddy currents in the iron cores are neglected in the mathematical model;
3) the stator end-winding effect and the rotor end-ring effect are considered by coupling the electrical circuits into the FEM equations;
4) to consider the skewed rotor bars, the motor in the axial direction is divided into M slices, with the rotor bars in each slice offset from each other by $(1/M)$th of the total skewing angle. In each slice the magnetic vector potential has an axial component only. Magnetic field is present only in planes normal to the machine axis. Hence the characteristic of the electromagnetic field of each slice is 2-D. The relationship between slices in the stator is based on the principle that the current flowing in the conductors of one slice is the same as that which flows in the same conductors of every other slice. Likewise, the relationship in the rotor is based on the principle that the network of the rotor cages should satisfy Kirchhoff's current and Kirchhoff's voltage laws.

The basic equations in the domains of iron core, air-gap, and stator conductor are the same as the corresponding 2-D multislice model. For the sake of completeness, these equations will be summarized below as well.

In Iron Cores and Air-gap Domains

According to the stated assumptions, the field equation in the iron domains and in the air-gap is

$$\nabla \times (\nu \nabla \times A) = 0 \tag{1}$$

where A is the axial component of the magnetic vector potential and ν is the reluctivity of the material.

In Stator Conductor Domain

In the stator conductor domain, the field equation is

$$\nabla \times (\nu \nabla \times A) \mp \frac{i_S}{S} = 0 \tag{2}$$

where i_S is the stator phase current and S is the total cross-sectional area of one turn on one coil side. The "$\mp$" sign becomes "$-$" for the "go" side of the conductor and it becomes "$+$" for the "return" side of the conductor.

A stator circuit of one phase is shown in Fig. 1. The stator circuit equation of one phase is

$$e + R_1 i_S + L_\sigma \frac{di}{dt} = v_S \tag{3}$$

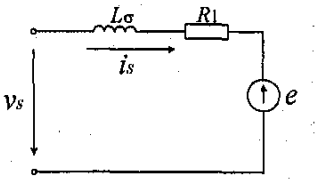

Fig. 1. A stator circuit of one phase.

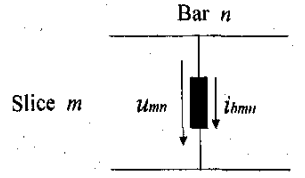

Fig. 2. A slice of rotor bar.

where R_1 is the total stator resistance of one phase winding and L_σ is the inductance of the end windings. The induced electromotive force is [9]

$$e = \frac{l_M}{S} \sum_{m=1}^{M} \left(\iint_{\Omega_m^+} \frac{\partial A}{\partial t} d\Omega - \iint_{\Omega_m^-} \frac{\partial A}{\partial t} d\Omega \right) \tag{4}$$

where the rotor is divided into an even number of M slices in the axial direction while m stands for the mth slice; $l_M = l/M$ and l is the axial length of the iron core; Ω^+ and Ω^- are, respectively, the cross-sectional areas of the "go" and "return" side of the phase conductors of the coils.

Substituting (4) into (3), the stator circuit equation is

$$\frac{l_M}{S} \sum_{m=1}^{M} \left(\iint_{\Omega_m^+} \frac{\partial A}{\partial t} d\Omega - \iint_{\Omega_m^-} \frac{\partial A}{\partial t} d\Omega \right) + R_i i_s + L_\sigma \frac{di_s}{dt} = v_s. \tag{5}$$

The field equation (2) and the circuit equation (5) can be combined to give rise to the basic formulas in the stator conductor domain. Here v_S is the exciting source, A and i_S are the unknowns.

In Rotor Conductor Domain

The Maxwell's equations applied to the domain in the nth bar of the mth slice (Fig. 2) will give rise to the following:

$$\nabla \times (\nu \nabla \times A) + \sigma \frac{\partial A}{\partial t} - \frac{\sigma}{l_M} u_{mn} = 0 \tag{6}$$

where u_{mn} is the voltage between the two terminals of the nth bar on the mth slice.

The total current in the nth bar of the mth slice is

$$i_{bmn} = \sigma \left(\iint_{\Omega_{mn}} \left(-\frac{\partial A}{\partial t} + \frac{u_{mn}}{l_M} \right) d\Omega \right). \tag{7}$$

A network of the rotor cage is shown in Fig. 3. For normal operating frequencies (i.e., 50 or 60 Hz), the inductive component of the interbar impedance can be neglected [11].

Authorized licensed use limited to: Hong Kong Polytechnic University. Downloaded on March 14, 2009 at 10:34 from IEEE Xplore. Restrictions apply.

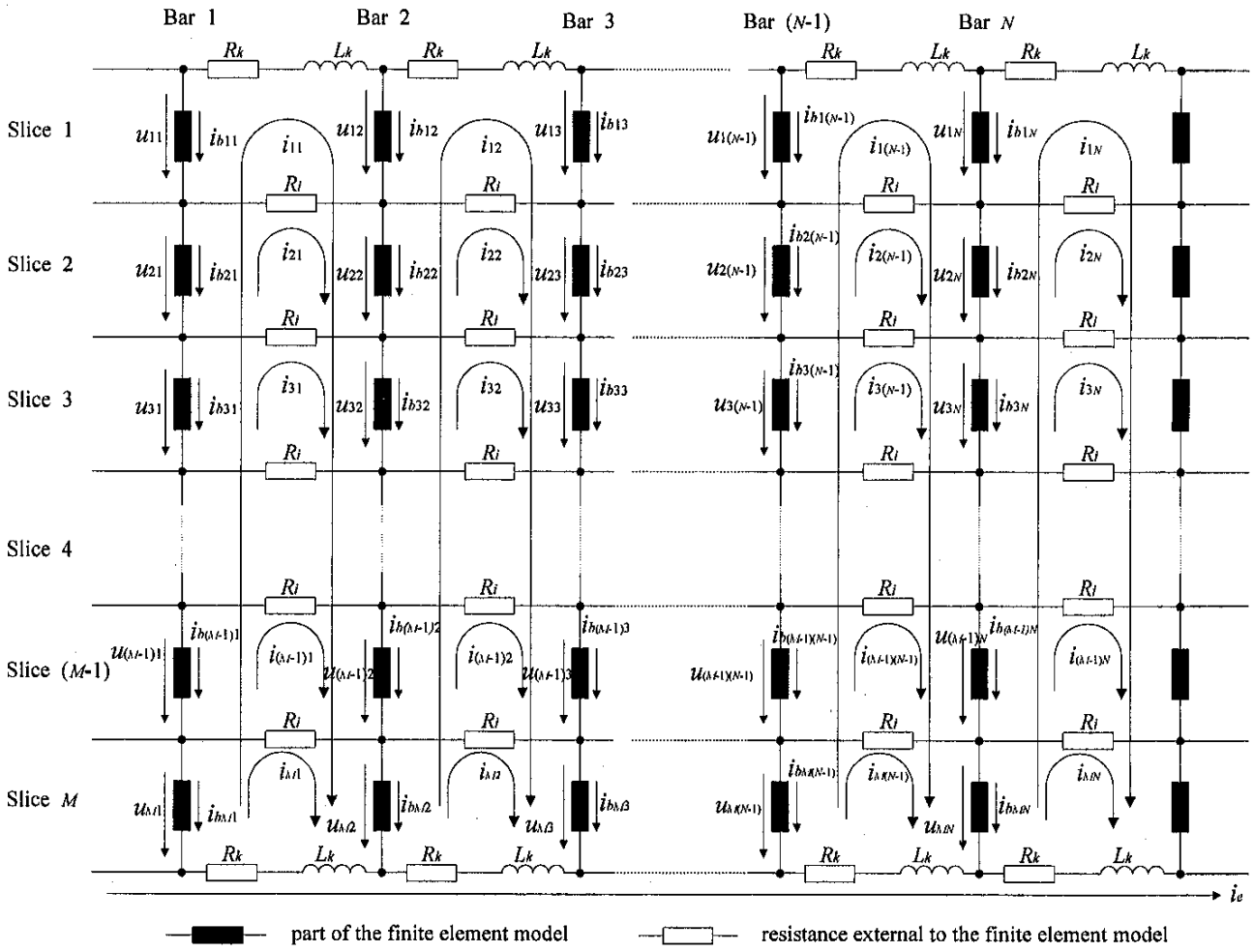

Fig. 3. Equivalent circuit for a rotor cage network.

Two adjacent bars are connected by the end-ring resistances and inductances at the two end rings as well as by the interbar resistances along the axial length of the rotor. The end-ring impedances can be computed using traditional methods or 3-D FEM [12], [13]. The interbar resistance can be determined according to [14] and [15]. Depending on whether the selected solution domain is spanning one pair of pole pitch or one pole pitch, bar 1 and bar $(N+1)$ can be connected, respectively, by virtue of the periodicity boundary condition or antiperiodic condition.

For a network of the rotor cage having M slices and N bars (Fig. 3), the graph has $(M+1)\times N$ nodes and $M\times N+(M+1)\times N$ branches. The current distribution can be specified in terms of $[M\times N+(M+1)\times N]-[(M+1)\times N]+1$ or $M\times N+1$ independent rotor currents. By tracing the loops for the mesh currents in the clockwise direction, the $M\times N$ mesh currents (labeled $i_{m1}, i_{m2}, \ldots, i_{mN}, m=1,\ldots,M$) used to describe the circuits are as shown in Fig. 3. The merit of this choice is that even if the interbar currents are ignored, the proposed method is still applicable. Another independent current is a circulating current i_e in one of the end rings. For an induction motor with two complete end rings, the application of Kirchhoff's voltage law around two end rings and each loop of interbars (the loop is between the two adjacent slices parallel to the end rings) will give rise to $i_e=0$. This will immediately reduce the number of unknown rotor currents by one.

The branch currents of the rotor bars can be expressed as

$$\begin{bmatrix} i_{hm1} \\ i_{hm2} \\ i_{hm3} \\ \vdots \\ i_{hmN} \end{bmatrix} = -\begin{bmatrix} 1 & 0 & 0 & & \mp 1 \\ -1 & 1 & 0 & & 0 \\ 0 & -1 & 1 & \cdots & 0 \\ & & \vdots & \ddots & \\ 0 & 0 & & -1 & 1 \end{bmatrix} \begin{bmatrix} i_{11} \\ i_{12} \\ i_{13} \\ \vdots \\ i_{1N} \end{bmatrix} - K\begin{bmatrix} 1 & 0 & 0 & & \mp 1 \\ -1 & 1 & 0 & & 0 \\ 0 & -1 & 1 & \cdots & 0 \\ & & \vdots & \ddots & \\ 0 & 0 & & -1 & 1 \end{bmatrix} \begin{bmatrix} i_{m1} \\ i_{m2} \\ i_{m3} \\ \vdots \\ i_{mN} \end{bmatrix} \tag{8}$$

where $i_{11}, i_{12}, \ldots, i_{1N}$ and $i_{m1}, i_{m2}, \ldots, i_{mN}, (m=2,\ldots,M)$ are the mesh currents. When $m=1$, $K=0$. For $m>1$, $K=1$. If the domain to be investigated spans over one pair of poles, the "$\mp$" sign in (8) should be "$-$." If the studied domain is one pole, then the "$\mp$" sign should be "$+$."

Authorized licensed use limited to: Hong Kong Polytechnic University. Downloaded on March 14, 2009 at 10:34 from IEEE Xplore. Restrictions apply.

Substituting (8) into (7) one obtains the branch equations as

$$\sigma\left(\iint_{\Omega_{mn}}\left(-\frac{\partial A}{\partial t}+\frac{u_{mn}}{l_M}\right)d\Omega\right)+\begin{bmatrix}1&0&0&&\mp1\\-1&1&0&&0\\0&-1&1&\cdots&0\\&&\vdots&\ddots&\\0&0&&-1&1\end{bmatrix}\begin{bmatrix}i_{11}\\i_{12}\\i_{13}\\\vdots\\i_{1N}\end{bmatrix}+K\begin{bmatrix}1&0&0&&\mp1\\-1&1&0&&0\\0&-1&1&\cdots&0\\&&\vdots&\ddots&\\0&0&&-1&1\end{bmatrix}\begin{bmatrix}i_{m1}\\i_{m2}\\i_{m3}\\\vdots\\i_{mN}\end{bmatrix}=0 \quad (9)$$

where $m=1,2,\cdots,M$ and $n=1,2,\ldots N$. There are totally $M\times N$ branch equations.

The total number of $M\times N$ mesh-current equations can be further established by considering the loop $i_{11},i_{12},\ldots,i_{1N}$

$$\sum_{m=1}^{M}\begin{bmatrix}1&-1&0&\cdots&0\\0&1&-1&\cdots&0\\0&0&1&\cdots&0\\0&0&&\ddots&\\\mp1&0&0&\cdots&1\end{bmatrix}\begin{bmatrix}u_{m1}\\u_{m2}\\\vdots\\u_{mN}\end{bmatrix}+(-2R_k)I\begin{bmatrix}i_{11}\\i_{12}\\\vdots\\i_{1N}\end{bmatrix}+(-2L_k)I\begin{bmatrix}\frac{di_{11}}{dt}\\\frac{di_{12}}{dt}\\\vdots\\\frac{di_{1N}}{dt}\end{bmatrix}+(-R_k)I\begin{bmatrix}i_{M1}\\i_{M2}\\\vdots\\i_{MN}\end{bmatrix}+(-L_k)I\begin{bmatrix}\frac{di_{M1}}{dt}\\\frac{di_{M2}}{dt}\\\vdots\\\frac{di_{MN}}{dt}\end{bmatrix}=0 \quad (10)$$

where R_k, L_k are the resistance and inductance of the rotor end rings, respectively. I is a $N\times N$ unit diagonal matrix.

For the loop $i_{m1},i_{m2},\ldots,i_{mN}$ $(m=2,\ldots,M-1)$

$$\begin{bmatrix}1&-1&0&\cdots&0\\0&1&-1&\cdots&0\\0&0&1&\cdots&0\\0&0&1&\cdots&0\\0&0&&\ddots&\\\mp1&0&0&\cdots&1\end{bmatrix}\begin{bmatrix}u_{m1}\\u_{m2}\\\vdots\\u_{mN}\end{bmatrix}+KR_iI\begin{bmatrix}i_{(m-1)1}\\i_{(m-1)2}\\\vdots\\i_{(m-1)N}\end{bmatrix}+(-2R_i)I\begin{bmatrix}i_{m1}\\i_{m2}\\\vdots\\i_{mN}\end{bmatrix}+R_iI\begin{bmatrix}i_{(m+1)1}\\i_{(m+1)2}\\\vdots\\i_{(m+1)N}\end{bmatrix}=0 \quad (11)$$

where R_i is the interbar resistance. When $m=2$, $K=0$. If $m>2$, then $K=1$.

For the loop $i_{M1},i_{M2},\ldots,i_{MN}$

$$\begin{bmatrix}1&-1&0&\cdots&0\\0&1&-1&\cdots&0\\0&0&1&\cdots&0\\0&0&1&\cdots&0\\0&0&&\ddots&\\\mp1&0&0&\cdots&1\end{bmatrix}\begin{bmatrix}u_{M1}\\u_{M2}\\\vdots\\u_{MN}\end{bmatrix}+(-R_k)I\begin{bmatrix}i_{11}\\i_{12}\\\vdots\\i_{1N}\end{bmatrix}+(-L_k)I\begin{bmatrix}\frac{di_{11}}{dt}\\\frac{di_{12}}{dt}\\\vdots\\\frac{di_{1N}}{dt}\end{bmatrix}+R_iI\begin{bmatrix}i_{(M-1)1}\\i_{(M-1)2}\\\vdots\\i_{(M-1)N}\end{bmatrix}+(-R_k-R-i)I\begin{bmatrix}i_{M1}\\i_{M2}\\\vdots\\i_{MN}\end{bmatrix}+(-L_k)I\begin{bmatrix}\frac{di_{M1}}{dt}\\\frac{di_{M2}}{dt}\\\vdots\\\frac{di_{MN}}{dt}\end{bmatrix}=0. \quad (12)$$

The magnetic field equation (6) together with the branch equation (9) and the mesh-current equations (10)–(12) will give rise to the basic governing formulas in the rotor conductor domain.

III. Global System Equations

The potential can be expressed as the sum of the shape functions times the nodal potential

$$A=\sum_{i=1}^{M_e}N_iA_i \quad (13)$$

where there are M_e nodes in the element and N_i are the shape functions.

Using the Galerkin method, one has the intergral equations of the field problems. In the iron cores and air-gap domains associated with (1), one has

$$\iint_{\Omega}\left[\frac{\partial N_i}{\partial x}\frac{\partial}{\partial x}\nu\sum_{j=1}^{M}N_jA_j+\frac{\partial N_i}{\partial y}\frac{\partial}{\partial y}\nu\sum_{j=1}^{M}N_jA_j\right]d\Omega=0. \quad (14)$$

In the stator conductor domains associated with (2), one has

$$\iint_{\Omega}\left[\frac{\partial N_i}{\partial x}\frac{\partial}{\partial x}\nu\sum_{j=1}^{M}N_jA_j+\frac{\partial N_i}{\partial y}\frac{\partial}{\partial y}\nu\sum_{j=1}^{M}N_jA_j+N_i\left(\mp\frac{i_s}{S}\right)\right]d\Omega=0. \quad (15)$$

In the rotor bar domains associated with (6), one has

$$\iint_{\Omega}\left[\frac{\partial N_i}{\partial x}\frac{\partial}{\partial x}\nu\sum_{j=1}^{M}N_jA_j+\frac{\partial N_i}{\partial y}\frac{\partial}{\partial y}\nu\sum_{j=1}^{M}N_jA_j+\sigma N_i\frac{\partial}{\partial t}\sum_{j=1}^{M}N_jA_j-N_i\left(\frac{\sigma}{l_M}u_{mn}\right)\right]d\Omega=0. \quad (16)$$

Authorized licensed use limited to: Hong Kong Polytechnic University. Downloaded on March 14, 2009 at 10:34 from IEEE Xplore. Restrictions apply.

Discretizing (14)–(16), (5), (9), and coupling (10)–(12) together, one obtains the following global system equations:

$$\begin{bmatrix} C_{11} & C_{12} & C_{13} & 0 \\ 0 & C_{22} & 0 & 0 \\ 0 & 0 & C_{33} & C_{34} \\ 0 & 0 & C_{43} & C_{44} \end{bmatrix} \begin{bmatrix} A \\ i_S \\ u \\ i_R \end{bmatrix} + \begin{bmatrix} D_{11} & 0 & 0 & 0 \\ D_{21} & D_{22} & 0 & 0 \\ D_{31} & 0 & 0 & 0 \\ 0 & 0 & 0 & D_{44} \end{bmatrix} \begin{bmatrix} \frac{\partial A}{\partial t} \\ \frac{\partial i_S}{\partial t} \\ \frac{\partial u}{\partial t} \\ \frac{\partial i_R}{\partial t} \end{bmatrix} = \begin{bmatrix} 0 \\ P_2 \\ 0 \\ 0 \end{bmatrix} \quad (17)$$

where the first line of the submatrix is the magnetic field equations; the second line is the stator circuit equations; the third line is the branch equations of the rotor bars; the last line is the mesh-current equations of the rotor network. The unknowns $[A]$ are the magnetic vector potentials; $[i_S]$ are the stator phase currents; $[u]$ are the voltages of the rotor bars on each slice, and $[i_R]$ are the mesh-currents in the rotor network.

The elements of the coefficient matrix are

$$C_{11ij} = \iint_{\Omega_e} \nu \left(\frac{\partial N_i}{\partial x} \frac{\partial N_j}{\partial x} + \frac{\partial N_i}{\partial y} \frac{\partial N_j}{\partial y} \right) d\Omega \quad (18)$$

$$D_{11ij} = \iint_{\Omega_e} \sigma N_i N_j \, d\Omega \quad (19)$$

i and j are the node numbers in (18) and (19). In the iron cores as well as in the air-gap and stator conductors, $D_{11ij} = 0$

$$C_{12ij} = \mp \frac{1}{S} \iint_{\Omega_j} N_i \, d\Omega \quad (20)$$

$$D_{21ji} = \pm \frac{l_M}{S} \iint_{\Omega_j} N_i \, d\Omega. \quad (21)$$

i is the node number and j is the stator conductor number in (20) and (21). In (20), for the "go" side of the stator conductors, the "$\mp$" sign is "$-$" whereas it becomes "$+$" for the "return" side. In (21), for the "go" side of the stator conductors, the "$\pm$" sign is "$+$" whereas it becomes "$-$" for the "return" side. Moreover

$$C_{22} = [R_1 \quad R_2 \quad R_1]_{3\times 3}^{\text{diagonal}} \quad (22)$$

$$D_{22} = [L_\sigma \quad L_\sigma \quad L_\sigma]_{3\times 3}^{\text{diagonal}} \quad (23)$$

where C_{22} and D_{22} are 3×3 matrices associated with the three phases in the stator windings

$$C_{13ij} = - \iint_{\Omega_j} N_i \frac{\sigma}{l_M} \, d\Omega \quad (24)$$

$$D_{31ji} = - \iint_{\Omega_j} \sigma N_i \, d\Omega. \quad (25)$$

In (24) and (25), i is the node number and j is the rotor bar number of each slice

$$C_{33} = \left[\frac{\sigma S}{l_M} \quad \frac{\sigma S}{l_M} \quad \cdots \quad \frac{\sigma S}{l_M} \right]_{(M\times N)\times(M\times N)}^{\text{diagonal}} \quad (26)$$

where S is the area of the cross section of one rotor bar. The matrix C_{34} in (17) is given in (27) shown at the bottom of the page, and all the submatrix in (27) are the same as follows:

$$C_{34(11)} = \cdots = C_{34(M1)} = \cdots = C_{34(MM)} = \begin{bmatrix} 1 & 0 & 0 & & \mp 1 \\ -1 & 1 & 0 & & 0 \\ 0 & -1 & 1 & \cdots & 0 \\ & & \vdots & \ddots & \\ 0 & 0 & & -1 & 1 \end{bmatrix}_{(N\times N)} \quad (28)$$

In (28) the "$\mp$" sign should be "$-$" if the domain to be investigated spans over one pair of poles. It becomes "$+$" if the studied domain is one pole. Moreover,

$$C_{43} = C_{34}^T. \quad (29)$$

By virtue of the characteristics of (29), it is now possible to modify the global system equations to make them to become symmetrical as described below. See (30) shown at the bottom of the following page. Moreover

$$D_{44} = \begin{bmatrix} -2L_kI & 0 & 0 & & -L_kI \\ 0 & 0 & 0 & & 0 \\ 0 & 0 & 0 & & 0 \\ & & \vdots & \ddots & \\ -L_kI & 0 & 0 & & -L_kI \end{bmatrix}_{(M\times N)\times(M\times N)} \quad (31)$$

where C_{44} and D_{44} are symmetrical matrices with $M \times M$ submatrices; I is a $N \times N$ unit diagonal matrix.

The vector on the right-hand side is

$$P_2 = [v_A \quad v_B \quad v_C]^T \quad (32)$$

where v_A, v_B, and v_C are the three stator phase voltages.

$$C_{34} = \begin{bmatrix} C_{34(11)} & 0 & 0 & & 0 \\ C_{34(21)} & C_{34(22)} & 0 & & 0 \\ C_{34(31)} & & C_{34(33)} & \cdots & 0 \\ & & \vdots & \ddots & \\ C_{34(M1)} & 0 & 0 & 0 & C_{34(MM)} \end{bmatrix}_{(M\times N)\times(M\times N)} \quad (27)$$

Authorized licensed use limited to: Hong Kong Polytechnic University. Downloaded on March 14, 2009 at 10:34 from IEEE Xplore. Restrictions apply.

IV. Solution of System Equations

Using Backward Euler's method to discretize the time variable, one obtains the recurrence formulas of the kth step for the time stepping process as follows:

$$\begin{bmatrix} C_{11}^k + \frac{D_{11}^k}{\Delta t} & C_{11}^k & C_{13}^k & 0 \\ \frac{D_{21}^k}{\Delta t} & C_{22}^k + \frac{D_{22}^k}{\Delta t} & 0 & 0 \\ \frac{D_{31}^k}{\Delta t} & 0 & C_{33}^k & C_{34}^k \\ 0 & 0 & C_{43}^k & C_{44}^k + \frac{D_{44}^k}{\Delta t} \end{bmatrix} \begin{bmatrix} A^k \\ i_S^k \\ u^k \\ i_R^k \end{bmatrix} = \begin{bmatrix} 0 \\ P_2^k \\ 0 \\ 0 \end{bmatrix} + \frac{1}{\Delta t} \begin{bmatrix} D_{11}^k & 0 & 0 & 0 \\ D_{21}^k & D_{22}^k & 0 & 0 \\ D_{31}^k & 0 & 0 & 0 \\ 0 & 0 & 0 & D_{44}^k \end{bmatrix} \begin{bmatrix} A^{k-1} \\ i_S^{k-1} \\ u^{k-1} \\ i_R^{k-1} \end{bmatrix}. \tag{33}$$

Noting that

$$-\frac{\Delta t}{l_M}\left(\frac{D_{21ji}}{\Delta t}\right) = C_{12ij} \tag{34}$$

and

$$\frac{\Delta t}{l_M}\left(\frac{D_{31ji}}{\Delta t}\right) = C_{31ij} \tag{35}$$

where $C_{11}, D_{11}, C_{33}, C_{44}, D_{44}$ are symmetrical submatrices. By making use of the properties of (29) and multiplying $(-\Delta t/l_M)$ to the second rows of the submatrixes in (33), multipling $(\Delta t/l_M)$ to the third and fourth rows of the submatrixes in (33), the coefficient matrix of the system equations will become symmetrical.

After the mesh of each slice is generated, the nodes, elements, etc. in the FEM model are renumbered slice by slice continually. Therefore, the data structure of the resultant FEM becomes 2-D. The number of total unknown magnetic vector potentials is $NP \times M$ (where NP is the number of nodes with unknown magnetic vector potentials on one slice). In the stator conductor domains there are three unknown stator phase currents. Each stator conductor should be identified according to its phase location although one does not need to take care of which slice it belongs to. In the rotor conductor domain, there are $M \times N$ unknown branch voltages and $M \times N$ unknown mesh currents. Each rotor bar at the different slices should be identified because the rotor voltages of the various slices are different although they belong to the same bar.

The total number of unknowns are $NP \times M + 3 + M \times N + M \times N$. If the last $(M-1) \times N$ are unknowns, that is, the unknowns $i_{m1}, i_{m2}, \ldots, i_{mN}$ $(m = 2, \ldots, M)$, are not included in the system equations, the interbar currents will be neglected.

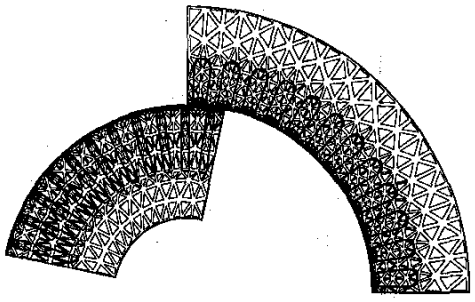

Fig. 4. Finite element mesh using triangles.

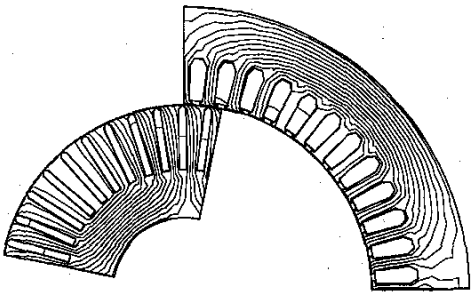

Fig. 5. Flux plot when the motor is in full load operation.

For steady-state problems, the complex network-field coupled multislice FEM model is solved first to give an initial guess of $A(0), i_S(0), u(0)$, and $i_R(0)$. At each time step, the Newton–Raphson method coupled with the incomplete Cholesky conjugate gradient (ICCG) algorithm are used to solve the system of large nonlinear equations.

During the time stepping process, the rotor FEM mesh is moved in accordance with the rotor movement. The mesh rotation techniques have already been reported in [9].

V. Example

The proposed network-field coupled FEM modeling has been used to simulate the steady-state operations of a skewed rotor induction motor (11 kW/380 V, 50 Hz, four poles, 48 stator slots, 44 rotor slots, Δ connection, rotor bars skew 1.3 stator slot pitch). The time step size is 0.038 ms. The solution domain of the FEM is one pole pitch. The 2-D FEM mesh of each slice has 1 626 nodes and 2 655 elements (Fig. 4). A typical flux plot is given in Fig. 5.

The computed interbar current losses with different slice numbers are listed in Table I. The CPU time given in Table I

$$C_{44} = \begin{bmatrix} -2R_kI & 0 & 0 & & -R_kI \\ 0 & -2R_iI & R_iI & & 0 \\ 0 & R_iI & -2R_iI & R_iI & 0 \\ & & \vdots & \ddots & \\ -R_kI & 0 & 0 & R_iI & -(R_k+R_i)I \end{bmatrix}_{(M\times N)\times(M\times N)} \tag{30}$$

Authorized licensed use limited to: Hong Kong Polytechnic University. Downloaded on March 14, 2009 at 10:34 from IEEE Xplore. Restrictions apply.

TABLE I
COMPARISON OF COMPUTED INTER-BAR LOSSES WHEN CHOOSING DIFFERENT SLICE NUMBER

Slice Number	Unknown Number	CPU Time (s)	Inter-bar loss (W)
1	1370	1.5	0.0
2	2737	4.9	25.9
3	4104	10.7	17.2
4	5471	18.5	15.1
5	6838	26.9	14.5
6	8205	36.3	13.6
7	9572	47.1	13.2
8	10939	57.6	12.9
9	12306	69.5	12.5

TABLE II
COMPARISON OF COMPUTED INTER-BAR CURRENT LOSSES WHEN USING 2-D FEM AND 3-D FEM (W)

2-D Network-field Coupled FEM	12.5
3-D FEM	10.8

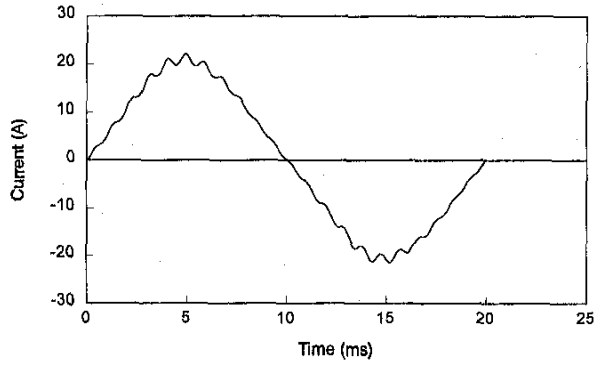

Fig. 6. Computed stator phase current waveforms at full-load operation.

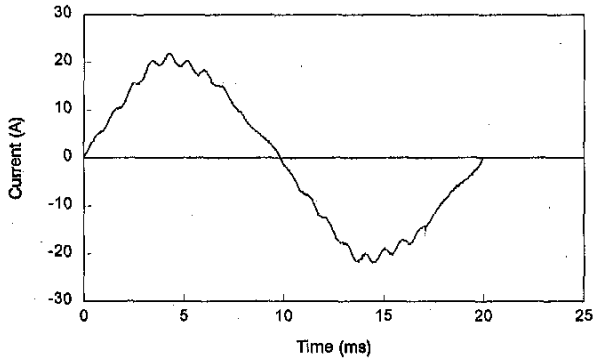

Fig. 7. Measured stator phase current waveforms at full-load operation.

is the average time to solve the system equations at each time step on a Pentium II/300 MHz. The comparison between the results using 2-D network-field coupled FEM and the 3-D FEM which has been reported by authors in [10] is given in Table II. It shows that in order to obtain an accurate estimation of the interbar loss with a 2-D model, the motor should be divided into about nine slices axially. A typical computed stator current waveform and the corresponding measured ones are shown in Figs. 6 and 7, respectively.

TABLE III
COMPARISON OF COMPUTED INTER-BAR LOSS WHEN THE ROTOR BARS SKEW DIFFERENT ANGLES

Skewed Angle of Rotor Bars	Inter-bar loss (W)
0.0 stator slot pitch	0.09
0.3 stator slot pitch	4.97
0.6 stator slot pitch	7.18
1.0 stator slot pitch	10.93
1.3 stator slot pitch	12.51
1.6 stator slot pitch	14.15

TABLE IV
COMPARISON OF COMPUTED AND MEASURED STRAY LOSSES (W)

	Computed	Tested
Eddy-current Stray Loss	135.9	
Hysteresis Stray Loss	7.6	
Stator Copper Stray Loss	2.7	
Rotor Copper Stray Loss	8.2	
Inter-Bar Current Loss	12.5	
Total	166.9	173.6

The developed 2-D modeling is also used to study the interbar current loss versus different skewing angles in the rotor bars. The computed results are in Table III. It can be seen that as the skew angle increases, the interbar current loss will also increase.

By using the time stepping method, one can obtain the waveforms of currents and the distributions of the magnetic flux densities in the time domain with the proposed 2-D algorithm. These computed results can be further used to estimate the stray losses in the motor. The formulas which are required for estimating the stray losses are directly dependent on the actual changes of currents and magnetic flux densities waveforms as described by the authors [10]. The computed full-load results of the motor are shown in Table IV. The computed stray losses are very close to the tested results obtained by the reverse rotation method [16].

VI. CONCLUSION

The proposed multislice 2-D time stepping FEM model which includes the effect of skewing in the rotor bars is a further development of modeling induction machines. By coupling the rotor cage network circuits into the field equations, one can include an analysis of an essentially 3-D interbar currents in the proposed 2-D model. In addition, the model can take into account the other difficult problems such as eddy-currents, saturation, and rotor movement, as well as other nonsinusoidal quantities directly in the system equations. The method has resulted in a large reduction in computing time when solving an essentially 3-D problem. It will provide a powerful tool for studying the behavior of electric machines, especially when the effects of skewing in the rotor bars as well as interbar currents are to be included.

REFERENCES

[1] S. L. Ho and W. N. Fu, "Review and further application of finite element methods in induction motors," *Electric Machines Power Syst.*, vol. 26, no. 2, pp. 111–125, 1998.

Authorized licensed use limited to: Hong Kong Polytechnic University. Downloaded on March 14, 2009 at 10:34 from IEEE Xplore. Restrictions apply.

[2] S. Williamson, "Induction motor modeling using finite elements," presented at the Int. Conf. Elect. Machines, Paris, France, Sept. 5–8, 1994, pp. 1–8.
[3] S. J. Salon, *Finite Element Analysis of Electric Machines*. Norwell, MA: Kluwer, 1995.
[4] A. Arkkio, "Analysis of induction motors based on the numerical solution of the magnetic field and circuit equations," *Helsinki, Acta Polytechnica Scandinavica, Elect. Eng. Series*, no. 59, pp. 1–66, 1987.
[5] S. Williamson, T. J. Flack, and A. F. Volschenk, "Representation of skew in time-stepped two-dimensional finite-element models of electrical machines," presented at the IEEE Ind. Applicat. Soc. Annual Meeting, Denver, CO, Oct. 1994.
[6] F. Piriou and A. Razek, "A model for coupled magnetic-electric circuits in electric machines with skewed slots," *IEEE Trans. Magn.*, vol. 26, pp. 1096–1100, Mar. 1990.
[7] J. J. C. Gyselinck and J. A. A. Melkebeek, "Modeling of electric machines with skewed slots using the two dimensional finite element method: An efficient solving technique," *Syst. Anal. Modeling Simulation*, vol. 18–19, pp. 559–562, 1995.
[8] B. Boualem and F. Piriou, "Modeling of induction motor accounting for skewed slots effects," presented at the Inter. Conf. Elect. Machines, Paris, France, Sept. 5–8, 1994, pp. 699–704.
[9] S. L. Ho and W. N. Fu, "A comprehensive approach to the solution of direct-coupled multislice model of skewed rotor induction motors using time-stepping eddy-current finite element method," *IEEE Trans. Magn.*, vol. 33, pp. 2265–2273, May, 1997.
[10] S. L. Ho, W. N. Fu, and H. C. Wong, "Estimation of stray losses of skewed induction motors using coupled 2-D and 3-D time stepping finite element methods," *IEEE Trans. Magn.*, vol. 34, pp. 3102–3105, Sept. 1998.
[11] I. Kerszenbaum and C. F. Landy, "The existence of large interbar currents in three phase squirrel cage motors with rotor-bar and/or end-ring faults," *IEEE Trans. Power Appart. Syst.*, vol. 103, pp. 1854–1862, July 1984.
[12] J. P. Ducreux, "Computation of asynchronous machine and winding leakage reactance with 3-D field calculation around the end region," in *Proc. Int. Conf. Elect. Machines*, Paris, France, Sept. 5–8, 1994, pp. 333–336.
[13] R. De Weerdt and R. Belmans, "Squirrel cage induction motor end effects using 2-D and 3-D finite elements," *Elect. Machines Drives*, Durham, U.K., Sept. 11–13, 1995, no. 412, pp. 62–66.
[14] A. Odok, "Stray-load losses and stray torques in induction machines," *Trans. Amer. Inst. Elect. Eng.*, vol. 77, Pt. III, pp. 43–53, Apr. 1958.
[15] N. Christofides, "Origins of load losses in induction motors with cast aluminum rotors," *Proc. Inst. Elect. Eng.*, vol. 112, pp. 2317–2332, Dec. 1965.
[16] B. J. Chalmers and A. C. Williamson, "Stray losses in squirrel-cage induction motors-validity of the reverse-rotation test method," *Proc. Inst. Elect. Eng.*, vol. 110, pp. 1773–1777, Oct. 1963.

S. L. Ho was born in 1953. He received the B.Sc. and Ph.D. degrees in electrical engineering from the University of Warwick, U.K. in 1976 and 1979, respectively.

He is presently a Professor in the Department of Electrical Engineering, the Hong Kong Polytechnic University, Kowloon, Hong Kong. He holds several patents and has published over 100 papers in journals and in leading conferences. His main research interests include the application of finite elements in electrical machines, phantom loading of machines, as well as the design and development of novel machines.

Dr. Ho is a member of both the Institution of Electrical Engineers of the U.K. and the Hong Kong Institution of Engineers.

H. L. Li was born in 1962 in Hunan, China. She received the B.Eng. and M.Eng. degrees in electrical engineering from Hunan University and Shanghai University of Technology, China, in 1982 and 1988, respectively.

She joined the Shanghai Institute of Electric Power as a Lecturer and is now a Research Assistant at the Hong Kong Polytechnic University. She has published about 20 papers in journals and international conferences. Her research interests include computer-aided design of electric machines, electromagnetic field computation, automatic control of electric machines, and development on novel permanent magnet motors.

W. N. Fu was born in 1961 in Zhejiang, China. He received the B.Eng. and M.Eng. degrees in electrical engineering from Hefei University of Technology, China, and Shanghai University of Technology, China, in 1982 and 1989, respectively. He received the Ph.D. degree from the Hong Kong Polytechnic University, Hong Kong, in 1999.

He was with Shanghai University as a Lecturer and at present is a Research Associate at the Hong Kong Polytechnic University. He has published over 50 papers in journals and international conferences. His research interests include electromagnetic field computation, motor control, and design and development of novel machines.

Authorized licensed use limited to: Hong Kong Polytechnic University. Downloaded on March 14, 2009 at 10:34 from IEEE Xplore. Restrictions apply.